

# Experimental Verification and Simulation Analysis of a Battery Directly Connected DC-Microgrid System

Ke Liu<sup>1,\*</sup>, Hirohito Yamada<sup>1,2</sup>, Katsumi Iwatsuki<sup>2</sup>, and Taiichi Otsuji<sup>2</sup>

<sup>1</sup>Graduate School of Engineering, Tohoku University, Sendai, Japan

<sup>2</sup>International Research Institute of Disaster Science, Tohoku University, Sendai, Japan

Email: liu.ke.t1@dc.tohoku.ac.jp (K.L.), hirohito.yamada.c1@tohoku.ac.jp (H.Y.),

katsumi.iwatsuki.e5@tohoku.ac.jp (K.I.), taiichi.otsuji.e8@tohoku.ac.jp (T.O.)

**Abstract**—The transformation towards renewable and sustainable energy, as well as the digitalization of energy, has promoted the development of the power system towards miniaturization, decentralization, and intelligence. As a solution, a battery-directly-connected DC microgrid has been proposed in previous studies for autonomous and decentralized coordination control (ADCC). We constructed a testbed of the battery directly connected DC-microgrid in our university campus which has been operating stably for more than one year. This study experimentally verifies the feasibility of the battery-directly-connected DC microgrid, and the process of autonomous, decentralized, and coordinated energy distribution between the distributed small batteries through power loading experiments. In addition, a simulator for analyzing the behavior of the DC microgrid test platform is built in MATLAB/Simulink, and its accuracy is verified based on an energy flow analysis, revealing its potential for cyber-physical-system (CPS) construction.

**Index Terms**—DC microgrid, off-grid, battery-directly-connected, autonomous-decentralized-cooperative-control

## I. INTRODUCTION

With the advancement of the Sustainable Development Goals (SDGs) set by the United Nations, the transition to renewable and sustainable energy and the digital transformation of energy have become key perspectives [1]. In such an opportunity, the DC microgrid that supports the integration of a large amount of distributed renewable energy has become an alternative solution for accommodating renewable energy.

In the past decade, the field of control strategies for DC microgrids has attracted widespread attention, and various advanced control algorithms have been developed to stabilize DC systems and optimize various objectives. In the multilevel control of microgrids [2], primary control is mainly responsible for local tasks completed by DC/DC converters, including voltage regulation, load allocation, and safety protection. The second level of control mainly regulates voltage fluctuations and

deviations. The control schemes involved are mainly divided into three types: centralized control, decentralized control, and distributed control [3–5]. Among them, centralized control, which requires a central control unit, has been widely studied although it's a weaker ability to deal with faults or disasters, while decentralized control is relatively stronger in this regard, but has limited global control capability. On the other hand, distributed control is somewhere in between, and seems to be a good choice, but communication networks need to be established, and higher requirements are imposed on the control technology. In our previous studies, an autonomous decentralized coordination control (ADCC) method was proposed based on a battery-directly-connected DC-microgrid system, which has demonstrated superior capabilities [6]. This scheme belongs to the fusion of primary control and second-level control, as it can achieve basic power distribution and voltage regulation in a simple way without the need for a DC/DC converter in the energy storage unit.

Autonomy means that no additional control unit is needed (such as conventional droop control based DC/DC converters), and the direction and magnitude of power flow are only decided by the voltage deference and resistances based on Ohm's law. Compared with conventional DC microgrids that place a large-capacity battery in one location, distributing multiple small batteries along the DC bus can provide a stronger electrical inertia force. When a power load consumes power, multiple batteries can work together to supply power to the load. In this scheme, additional communication lines do not be needed to communicate each battery with each other to autonomously allocate energy. This scheme is proposed as the first-level control scheme in reference [7], and centralized control will also be needed in the second level to achieve global optimization and further improve the partial optimization achieved by the ADCC scheme. Currently, the feasibility of this ADCC scheme has been verified in simulation in terms of the stability of the DC bus voltage. The DC bus voltage is set to 380 V or 400 V, considering transmission efficiency, load capacity, and the safety of low currents [8–10].

Manuscript received March 7, 2023; revised May 18, 2023; accepted June 16, 2023.

\*Corresponding author

Although connecting batteries directly to the DC bus has various advantages, including supplying strong electrical inertia force and reducing control delays, stability, and safety issues are likely to arise during actual operation, including voltage fluctuations and the risk of overcharging the battery [11–14]. Especially in the case of lithium-ion batteries, overcharging can cause thermal runaway, leading to fires and even explosions. In addition, although most lithium-ion batteries now have built-in BMS systems to prevent over-discharging, there is still a risk of fire if the battery is not stored properly. Therefore, ensuring the stable operation of the battery directly connected DC microgrid system is a crucial consideration.

The main work of this paper is to build and verify the stability of the battery directly connected DC-microgrid system in experiments and to analyze its performance through power loading experiments. Although our goal is to construct DC microgrids with a higher voltage of around 400 V, the DC bus constructed in the experiment is around 52 V considering safety, equipment cost, and equipment adaptability [15]. In addition, a simulator based on this test bed system will also be constructed to reproduce the energy distribution in the test platform. Its accuracy will also be verified by comparing it with experimental data, to validate the possibility of using this simulator as a cyber-physical system (CPS) in the future.

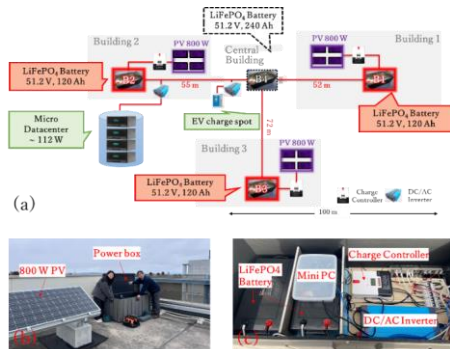


Fig. 1. A testing platform for a DC microgrid system: (a) Schematic diagram of the battery directly connected DC microgrid system, (b) PV-battery system at the roof of Building 2, and (c) The equipment configuration in the box.

## II. CONSTRUCTION OF A BATTERY DIRECTLY CONNECTED DC MICROGRID TESTBED

A testing platform for a DC microgrid system has been constructed in our university campus site (at Sendai, Japan), where multiple small batteries are distributed and directly connected to the DC bus as shown in Fig. 1(a). The system has been stably operating for more than one year. 16-cell LiFePO<sub>4</sub> batteries whose cell voltage is 3.2 V are directly connected to the DC bus at several points. Therefore, the DC bus voltage at the connecting points is equal to the terminal voltage of the batteries (rated voltage: 51.2 V).

The constructed microgrid is an off-grid system powered by renewable solar energy consisting of a total rated output power of 2.4 kW solar panels (PVs), a total storage capacity of 30 kWh batteries, and DC/AC inverters. The topology of the DC bus is a T-shape with the central building as the hub. Three buildings located at

the end of the DC bus are each equipped with solar panels with 800 W output and 120 Ah (6 kWh) storage capacity batteries on the rooftop of the buildings. The central building as the hub has the biggest battery of 240 Ah (12 kWh). The DC bus is constructed by 14 SQ CV cables. These four batteries are named with corresponding names of B1 to B4 according to their building name. To prevent overcharging of batteries, the PV charging operation is switched to float mode when the terminal voltage of the batteries reaches 55.2 V and the maximum disconnect voltage is set as 56 V. As for the over-discharge protection measures of the batteries, it is set to stop discharging when the voltage drops to 48 V. Due to the direct connection of the battery, the control strategy has been simplified. This means that apart from the rate control of charging and discharging of the battery to prevent overcharging and over-discharging during the conversion of photovoltaic power into stored electrical energy at the charging controller, there is no need for any control of the charging and discharging of the battery within the system because the process of charging and discharging the battery occurs spontaneously according to Ohm's law during the balancing of the voltage distribution of the battery terminals connected to the same bus within the system. As for the power load, a DC/AC inverter is installed on the roof of each building. A micro data center including four micro-servers is running on the rooftop of Building 2, consuming about 112 W of power at any time (without the cooler system in operation whose power is about 300 W). When the battery charging state is high and the power generation is sufficiently high for power consumption, electric vehicle charging (about 1.5 kW) will be carried out irregularly from the central building.

To monitor the operational status of the system, important information such as the amount of PV power generation, battery terminal voltage, and equipment temperature generated during the system operation is transmitted to a mini PC located nearby through the charge controller device every minute, and then remotely monitored through the communication network connected. The equipment specifications selected for this system are shown in Table I.

TABLE I: SPECIFICATIONS OF MAIN DEVICES IN THE BATTERY DIRECT CONNECTED DC OFF-GRID TESTBED

Device	Characteristic	Quantity
Solar Panel (PV)	Rated output power: 200 W Maximum output voltage: 36.9 V	12
LiFePO <sub>4</sub> Battery	Rated Voltage: 51.2 V Capacity: 60 Ah Equipped with BMS	10
DC/AC Inverter	Input Voltage: DC 48 V Output Voltage: AC 100 V, 50 Hz Maximum output power: 3 kW	2
	Input Voltage: DC 48 V Output Voltage: AC 100 V, 50 Hz Maximum output power: 1.5 kW	2
Charge Controller	PV side : DC 50 V (25°C) Battery side: DC 48 V Maximum output power: 3200W	3
Mini PC	CPU Intel® Celeron® J4125 8GB RAM+128GB SSD	3

The photo of the distributed PV-battery system located on the roof of B2 is shown in Fig. 1(b), where the battery, DC/AC inverter, mini PC, and other equipment are unified in the power box (the equipment configuration in the box is shown in Fig. 1(c)). Since the power box is located outdoors, it gets hot in the summer due to the direct radiation of sunlight, so it is equipped with an air cooling system. It also has an anti-freeze heater to prevent damage to the batteries because winter in Sendai often falls below freezing.

Currently, as a sufficient amount of power load is not connected to the microgrid and cannot match the total power generation of the microgrid, the system operates as an off-grid without being connected to the utility grid, resulting in surplus power. So far, there has been no shortage of power.

Fig. 2 shows the changes in PV power generation, battery terminal voltage, and the state-of-charge (SoC) of the battery measured in each building during January 2023. The PV power generation showed a relatively consistent daily amount of solar radiation in Sendai City, with occasional dips in power generation due to cloudy or snowy weather. Most of the time, the PV system was able to maintain a maximum power output of approximately 800 W. Throughout the day, the terminal voltage (equivalent to the DC bus voltage at the connection point) increased due to PV power generation, reaching its upper limit of 56 V on certain days (such as on the 4th, 5th, and 9th), but gradually decreasing from afternoon to evening due to the reduced charging current at the PV and the polarization phenomenon of the battery. In addition, the DC bus voltage decreased because of power consumption such as electric vehicle charging (e.g., from the 17th to the 20th). As a result, the DC bus voltage fluctuated between 51 V to 56 V, depending on solar radiation and power load usage, but remained within  $\pm 8\%$  of the standard value of 52 V.

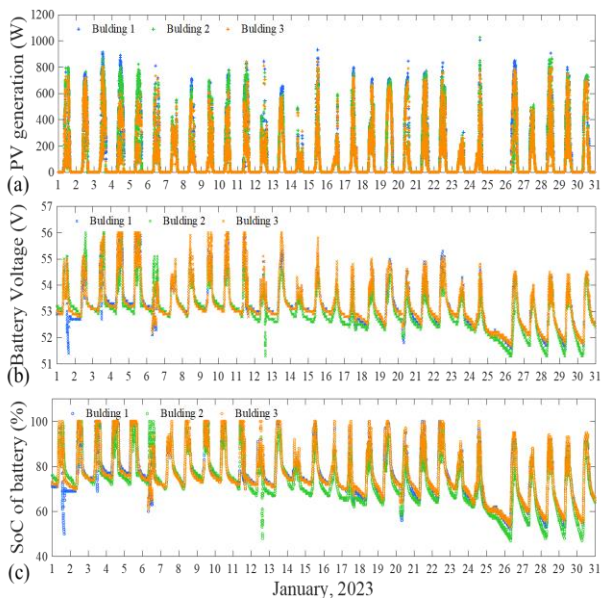


Fig. 2. Changes of the battery measured in each building during January 2023: (a) PV power generation, (b) battery terminal voltage, and (c) the state-of-charge (SoC).

In Fig. 2(c), the SoC of the battery shows a consistent trend with the DC bus voltage. The SoC here is calculated based on a pre-set value in the charge controller. When the voltage is around 54.8 V, the battery is considered fully charged (100%), and when it is around 48 V, the SoC is approximately 2%. Therefore, the remaining capacity of the battery can be roughly estimated based on the DC bus voltage.

The battery in each building was connected to the DC bus, which allowed for spontaneous power exchange between the batteries and ensured that the SoC of all batteries was balanced during the nighttime. It is worth noting that despite the voltage balance of the battery during nighttime, the terminal voltage of B2 remains relatively low (with a deviation of approximately 0.1 V to 0.2 V), due to a constant load consumption at B2 (the data center). Although the PV power generation was not high in January, there was little power consumption from loads other than electric vehicle charging or discharge experiments, so the battery SoC remained high throughout the month. In the latter half of the month, the battery voltage decreased significantly compared to the beginning of the month due to the severe weather condition. Particularly on the 25th, PV power generation was low due to weather conditions resulting in a relatively large drop in voltage of approximately 1 V.

### III. POWER LOADING TEST OF THE MICROGRID SYSTEMS

As mentioned in the previous section, since there is currently no household load connected to this system, this chapter conducted a power loading experiment to observe the autonomous coordinated power supply response of the system under different power loads. Specifically, considering the differences in power supply capacity between the central battery and the other batteries, B4 and B2 are prioritized as the targets for experimentation and evaluation in this study.

For B4, since the central building is not equipped with a solar power generation system, its power source is entirely obtained from the DC bus (or from other batteries). At the same time, as the hub of the system and the midpoint of the voltage, B4 has the largest battery capacity in the entire system (about 12 kWh). Therefore, when B4 experiences a load, its performance will be the first to be explored. The electronic load equipment connected to B4 in the central building has a maximum load power of 2.4 kW. Here, considering the response time of the battery voltage, the electronic load power is switched in the range of 0 W to 2.0 kW at 10-minute intervals, with a total experiment time of 80 mins (electronics load power was switched 8 times at 0 W, 1.2 kW, 200 W, 800 W, 600 W, 2 kW, 1.5 kW, and 0 W). The changes in the voltage and current flow during this process are recorded as shown in Fig. 3. As the experiment started at 9:40 AM, under the prevailing sunlight conditions of the day, the PV system had already begun charging B1-B3 at an approximate power of 600 W (as shown in Fig. 3(a)). Consequently, the initial voltage of B1 to B3 should have been relatively high.

However, due to the power consumption of the data center located in B2 and the absence of a power generation source at B4, the initial voltage of each battery ( $V_{Bi,0}$ , where  $i=1, 2, 3, 4$  represent the battery number, and the  $i$  that appears later in the text mean the same thing for ease of description), at the start of the experiment followed the relationship of  $V_{B4,0} \approx V_{B2,0} < V_{B1,0} \approx V_{B3,0}$ , as shown in Fig. 3(b).

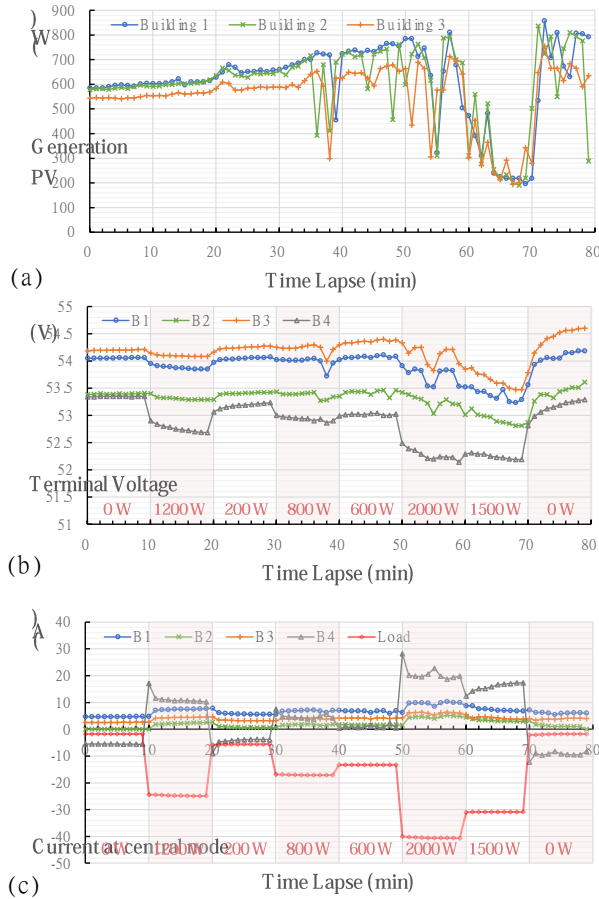


Fig. 3. Changes in the voltage and current flow: (a) PV power generation, (b) terminal voltage at B1-4, and (c) current flow at B4 on 9:40~11:00, April 14th, 2023, at Sendai, Japan.

Based on the voltage changes at each point on the DC bus (equivalent to the terminal voltage of each battery), it can be determined that when a load is connected to the DC bus, a voltage drop will occur at all points along the DC bus, and this voltage drop is in accordance with the discharge characteristics of the battery from fast to slow voltage change due to its polarization phenomenon. Since the electronic load is directly connected to B4, the voltage at the terminal of B4 undergoes the most dramatic change. Consequently, due to the voltage difference between B4 and other batteries, batteries B1 to B3 at higher potentials spontaneously coordinate to supply power to B4. The current changes at the central node (in front of B4) are monitored in the experiment, as shown in Fig. 3(c). In this case, the positive and negative current flows are defined as follows: the current flowing into the node in central is positive, and the current flowing out of the node is negative. The current magnitude of each

branch is related to the voltage difference and the resistance in the branch. Therefore, even though the potential at B3 is the highest, the current it provides is smaller than that of B1, due to the higher resistance between B3 and B4 compared to that between B1 and B4. At the same time, the resistance of each branch can be calculated through the cable length. However, in the case of short cable distances, the connection resistance cannot be ignored. Given the known voltage and current, the resistance at each branch ( $R_{Bi4}$ ) can also be determined by dividing the voltage difference between each battery by the current, i.e.,  $R_{Bi4} = |(V_i - V_4) / I_{i4}|$ ,  $i=1, 2, 3$ , where the  $V_i$  represents the terminal voltage of each battery and  $I_{i4}$  is the current flowing from each battery into B4. The resistance calculated by this formula shows some fluctuations due to the rapid voltage changes, but it can roughly estimate the magnitude relationship of the distributed resistance among the batteries as  $R_{B14} \approx R_{B24} \approx R_{B34} / 2$ , where  $R_{B14} \approx 160 \text{ m}\Omega$ .

Due to the limited voltage difference between each battery, with a maximum possible voltage difference of 8 V ((56–48) V), and the fixed resistance between the batteries, the coordinated current supply between batteries is also limited. In this experiment, the maximum voltage difference occurred when the power consumption was 2.0 kW, and the maximum current involved in the coordinated power supply was at the B1 branch with a current of around 10 A, equivalent to a discharge rate of 0.08 C. At this time, the voltage difference was 1.6 V. Therefore, it can be inferred that when the maximum voltage difference of 8 V occurs, the maximum discharge rate at each branch is only 0.42 C (50 A), which is an extreme case. Of course, due to real-time power-sharing operations, the voltage difference between batteries may not reach such a large value, and the actual current value will be much smaller than the limit value. It is worth noting that the continuous low-current charging operation also avoids the instant high-current charging operation, reducing damage to the batteries.

For B4, without considering a coordinated power supply, to provide an output power of 2.0 kW, its minimum output current ( $I_{B4,min}$ ) can be calculated as 38.3 A (corresponding to the B4 voltage of 52.2 V at a load of 2.0 kW in Fig. 3(b)), and this current value will continue to increase as the battery voltage decreases. However, when the battery supplies power to the DC load through a converter, the needed current at B4 ( $I_{B4,inv}$ ) will be higher than the minimum value  $I_{B4,min}$  due to the existence of conversion efficiency. If the efficiency of the converter is assumed to be 95%, the minimum current will be increased to 41.6 A, at which point the power losses will be approximately 105W. In the proposed ADCC system, according to Fig 3(c), B4 only needs to provide an average of 20 A and a maximum of 28.15 A to meet the demand. Besides, due to the small coordinated current, the loss caused by transmission is only about 3 W, which greatly improves the power supply capacity of a single battery. At the same time, it can also improve the voltage fluctuation in the battery when the load is connected. A load variation of 1.2 kW (from 0 W to 1.2 kW) at B4

caused a voltage drop of about 0.6 V within 10 min, and the maximum current during this process was about 17 A. When B4 is supplying this power alone, the voltage drop would be even greater. It can be estimated that when B4 is fully charged (56 V), it can provide a maximum power output of 16kW within ten minutes, and its current is only 227 A (0.95 C). Most importantly, this process occurs spontaneously.

Based on the autonomous coordinated power supply process described above, the power consumption of the electrical load at B4 can be satisfied. Fig. 4 illustrates the power source configuration and energy distribution process more visually. Negative values represent the process of charging B4. The non-zero load value is due to the power consumption required to maintain the electronic load and the operation of the inverter, which totals approximately  $100 \pm 10$  W.

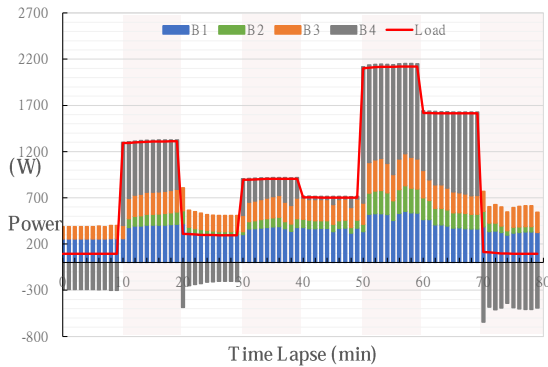


Fig. 4. Power supply composition when load consumption occurs at the B4.

The power supply sharing of each battery in Fig. 4 is calculated from the product of the terminal voltage and the current in Fig. 3. For battery B4, the power received from the other batteries is mainly used to balance the load when the load is heavy, whereas when the load is light, the excess power is not only used to supply the load but also used to balance the terminal voltage of B4, whose voltage has become lower due to previous discharge operation. It is worth noting that during the period of relatively stable voltage, the ratio of the coordinated power supply ( $P_{co}$ ) to the power provided by B4 ( $P_{B4}$ ) is always greater than 1.

Overall, the discharge experiment at B4 demonstrates the automatic coordinated power allocation capability of the battery direct connection system, as well as its advantages in improving the supply capacity of individual batteries and its easy control schemes.

Next, to investigate the performance of the battery (B2) located at the edge of the DC bus, we conducted a discharge experiment on B2 using the same electronic load equipment and operation during the same period. The total experiment time was 80 minutes, and the load power varied according to 8 values at intervals of 10 minutes (0 W, 1.2 kW, 200 W, 800 W, 600 W, 2 kW, 1.5 kW, and 0 W). Due to the presence of a solar power generation device, the actual load consumption after solar power generation balance is unpredictable. The PV power generation, the terminal voltage of each battery, and the

current value at the central node measured during the experiment are shown in Fig. 5.

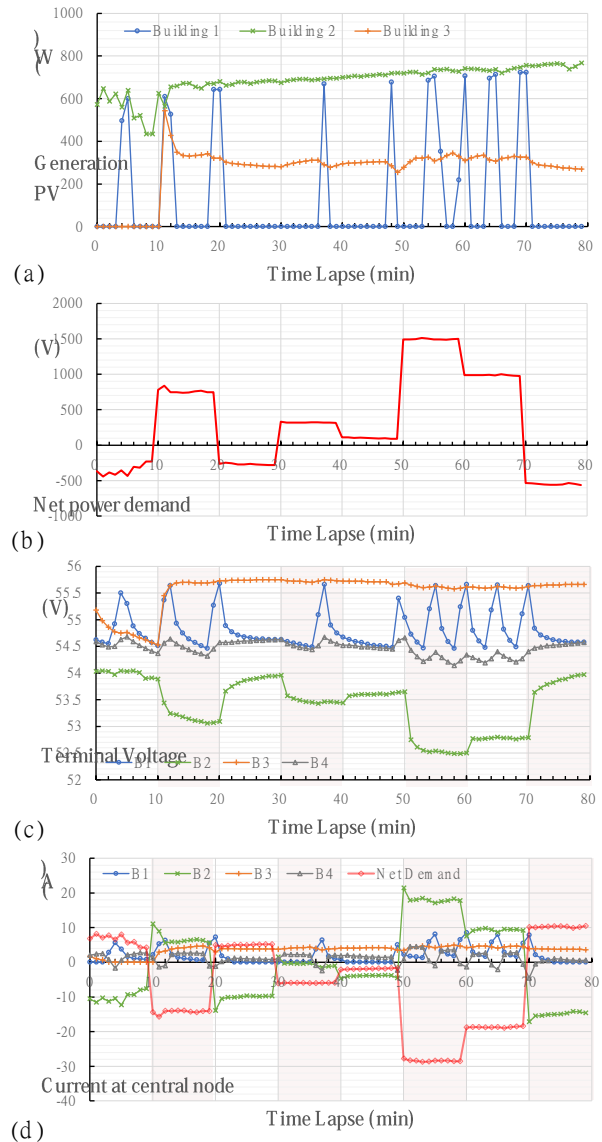


Fig. 5. Changes in (a) PV generation, (b) net power demand, (c) terminal voltage at B1-4, and (d) current flow at B4 on 9:40~11:00, April 22nd, 2023, at Sendai, Japan.

According to Fig. 5(a), due to sufficient power generation on the day, the PV system at B1 frequently switches between the idle mode (power generation is 0) and the MPPT charging mode. Corresponding to the trend of PV power generation, the terminal voltage at B1 also changes frequently under the polarization phenomenon. The PV system at B3 first enters the idle mode and then switches to the boost charging mode, suppressing the power generation, and thus keeping the terminal voltage at B3. This stage is set to last for 120 minutes. As for B2, due to the compensation of PV power generation, the maximum net demand for the system at B2 is only 1.5 kW. Currently, the net demand current is approximately 28 A, of which, according to Fig. 5 (d), around 10 A of current is obtained from other batteries. Therefore, B2 only needs to provide around 21.4 A to meet the net power demand. After the power demand increases from

200 W to 1.5 kW and continues to operate for ten minutes, the voltage drop of B2 reaches 1.2 V. This means that for a fully charged B2, it can operate at a maximum power of around 10 kW for 10 minutes, with a maximum operating current of approximately 143 A (1.2 C). Compared to a system without a coordinated power supply, where a fully charged (56 V) B2 can only provide a maximum of approximately 8 kW of instantaneous power under 143 A conditions, this proves that the coordinated power supply system also improves the power supply capacity of the battery at B2.

Furthermore, according to the power source configuration in Fig. 6 for B2, it can be observed that due to the persistently low potential at B2, coordination supply from other batteries to B2 occurs regardless of whether the net load demand is positive or negative. The net power demand represents the difference between the electricity consumption of electronic loads and the PV generation capacity. It is noteworthy that during the experiment, the maximum voltage difference between B2 and other batteries reached 3 V, while the maximum voltage difference during discharge at B4 was only 2 V. This is because the battery capacity at B2 is relatively small, making its voltage change more sensitive to load power.

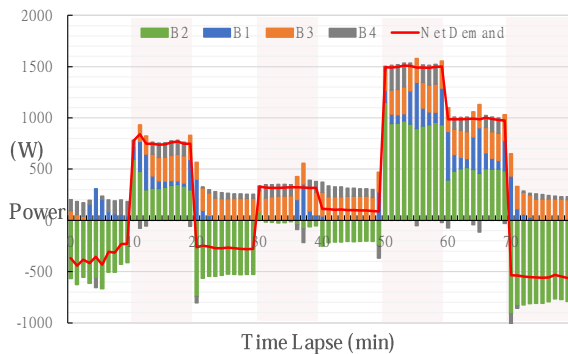


Fig. 6. Power supply composition when load consumption occurs at the B2.

And such a large voltage difference should have resulted in greater coordinated power, but due to the greater distribution resistance caused by the relatively large distance between B1 and B3 compared to B2, the ratio of the obtained coordinated power to the discharge power of B2 is between 0.5–1.5 when the voltage is relatively stable.

Overall, this experiment demonstrated that the proposed battery directly connected DC-microgrid system could implement autonomous, decentralized, and coordinated control of energy flow and power distribution.

#### IV. SIMULATOR CONSTRUCTION AND ANALYSIS

In previous research, the battery directly connected DC microgrid was proposed and studied its behavior with a simulator constructed on MATLAB/Simulink platform. However, the accuracy of the simulator still needs to be further validated due to the lack of comparison with experimental data.

Here, this work attempted to reproduce the behavior of the DC microgrid under the same conditions in the simulator. Considering the voltage value error that may measure at the charge controller, the changes in power flow caused by electric load fluctuation will be focused on simulation.

Fig. 7 shows the simulator interface which includes the PVs, batteries, different types of loads, and the DC bus connected to them as the main equipment. Each module was built based on real data such as the SQ and length of the CV cable used in the testbed, monitored PV generation power, measured battery discharge curve, and power consumption of given electrical loads (current source model). The partial parameters of the key models in the simulation are set in Table II. The internal resistance values of B1-B3 were measured using the current interruption approach method without the DC-bus connected [16], while the internal resistance of B4 is half that of the other three batteries because it is composed of two such batteries in parallel.

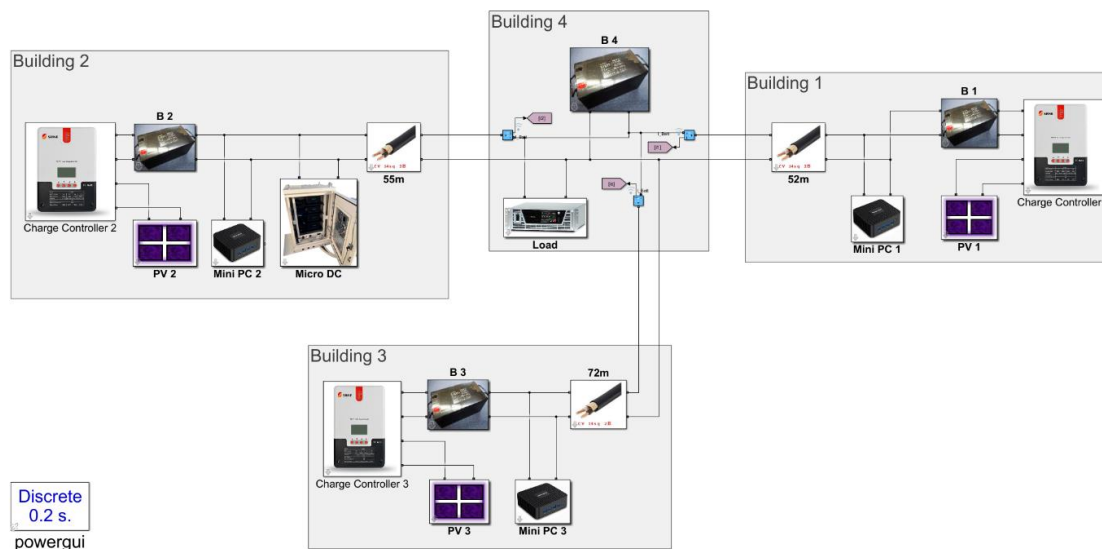


Fig. 7. Microgrid simulator interface based on battery direct connected DC bus.

TABLE II: SIMULATION PARAMETERS OF MAIN DEVICES

Device	Parameter	Value
PV	Generation power	Measured in experiment
Battery B1	Initial SoC	93%
	Internal Resistance	160 mΩ
Battery B2	Initial SoC (for experiment)	86%
	Internal Resistance	160 mΩ
Battery B3	Initial SoC	94%
	Internal Resistance	160 mΩ
Battery B4	Initial SoC	87%
	Internal Resistance	80 mΩ
MiniPC	Consumption Power	30 W
Micro data center	Consumption Power	112 W
DC/AC Inverter	Efficiency	92%
CV cable	Internal Resistance	1.71 Ω/km

The simulation step is set to 0.2 s, and the total duration is 80 minutes. The simulation results based on the simulator are recorded as shown in Fig. 6. The simulation curve has a certain width because the charge controller used to control the battery terminal voltage below 56V is a switching model that causes significant vibrations, but this does not affect the energy flow results.

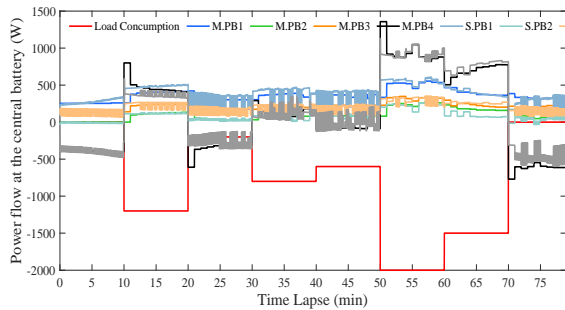


Fig. 8. Comparison of simulation results and experimental results with the variation of electric load power.

Comparing the simulated data with the measured data in Fig. 8, the power flow trend from B1 to B4 is always almost consistent, including the direction of power changes, the allocation ratio of power, and the response of the battery to changes in electric load power.

Although the transient change of battery power in the simulation was close to the experiment when the transient change of load power was small, the simulator was not able to restore the instantaneous power change accurately when the larger power change occurs. The largest power difference occurs at the last 1.5 kW change, and the difference between the two can reach about 500 W.

The reason for the discrepancy between the simulation results and the experimental data may be since the chemical reaction processes in the battery are not precisely reduced, and the effects due to battery polarization are yet to be described by a more accurate model. Besides, it may also be considered as the degradation of the battery model after long-term use. The precise modeling of batteries involving complex electrochemical reactions has always been a challenging field. However, overall, the simulation results for energy distribution are highly consistent with the experimental

results. Therefore, the simulator can be subsequently expected to be used to perform some experiments that are difficult to achieve in experiments, such as failure tests, load capacity tests, and other experiments. Furthermore, this also suggests that the simulator can be expected to be used as a CPS after further accurate modeling, the introduction of predictive data, etc.

## V. CONCLUSION

Based on the battery directly connected DC-microgrid testbed, this work conducted power loading experiments to analyze the performance and energy flow of the DC bus composed of battery terminal voltages. The study demonstrated that when a load unbalancing occurred in the bus-line, three batteries distributed in different locations could spontaneously and coordinately supply power, verifying the feasibility of implementing autonomous decentralized coordinated control based on the battery direct connection method. The proposed DC off-grid system has been stably and safely operating for about one year.

On the other hand, the high coincidence between the voltage curves and energy allocation of the simulator and the testing platform under the same power loading conditions validated the accuracy of the simulator. Although the simulator currently imports monitored solar energy generation data, it is foreseen that a simulator based on prediction data could implement functions such as based on predicted results (e.g., grid voltage and remaining battery capacity, etc.) and issue warning signals. Although this may be a relatively preliminary study in the work of constructing a CPS system, the work reveals the possibility of using this simulator for CPS systems in the future.

## CONFLICT OF INTEREST

The authors declare no conflict of interest.

## AUTHOR CONTRIBUTIONS

Ke Liu designed the research study, collected, and analyzed the data, and wrote the manuscript. Prof. Yamada contributed to the design of the study, analyzed the data, and revised the manuscript. Prof. Iwatsuki and Prof. Otsuji provided technical support and critical feedback on the manuscript. All authors have read and approved the final manuscript.

## FUNDING

This research was supported by JST OPERA Prog. (Grant Number JPMJOP1852) and JST SPRING (Grant Number JPMJSP2114).

## REFERENCES

- [1] R. M. Elavarasan, R. Pugazhendhi, T. Jamal *et al.*, "Envisioning the UN sustainable development goals (SDGs) through the lens of

energy sustainability (SDG 7) in the post-COVID-19 world,” *Applied Energy*, vol. 292, #116665, 2021.

- [2] M. Fotopoulou, D. Rakopoulos, D. Trigkas *et al.*, “State of the art of low and medium voltage direct current (DC) microgrids,” *Energies*, vol. 14, no. 18, #5595, 2021.
- [3] I. Federico, E. Jose, and F. Luis, “Master–slave DC droop control for paralleling auxiliary DC/DC converters in electric bus applications,” *IET Power Electronics*, vol. 10, no. 10, pp. 1156–1164, 2017.
- [4] G. Ensermu, A. Bhattacharya, and N. Panigrahy, “Real-time simulation of smart DC microgrid with decentralized control system under source disturbances,” *Arab J Sci Eng*, vol. 44, no. 8, pp. 7173–7185, 2019.
- [5] C. Teng, Y. Wang, F. Wang, and F. Zhang, “Distributed control strategy of hybrid energy storage system in the DC microgrid,” *The Journal of Engineering*, vol. 2019, no. 16, pp. 2851–2855, 2019.
- [6] K. Liu, H. Yamada, K. Iwatsuki, and T. Otsuji, “A study for stable operation of battery loaded DC bus based on autonomous cooperative control,” in *Proc. 2021 6th International Conference on Power and Renewable Energy*, Shanghai, China, 2021, pp. 1165–1168.
- [7] T. Otsuji, K. Iwatsuki, H. Yamada, and M. Yashima, “Concept of resilient electric power and information communication technology (R-EICT) converged network systems based on overall optimization of autonomous decentralized cooperative control of DC microgrids,” in *Proc. 2021 IEEE Power & Energy Society Innovative Smart Grid Technologies Conf.*, Washington, DC, USA, 2021, pp. 1–5.
- [8] M. Noritake, K. Yuasa, T. Takeda *et al.*, “Experimental study of a 400 V class DC microgrid for commercial buildings,” in *Proc. 2015 9th International Conf. on Power Electronics and ECCE Asia*, Seoul, Korea, 2015, pp. 1730–1735.
- [9] L. Li, K.-J. Li, K. Sun, Z. Liu, and W.-J. Lee, “A comparative study on voltage level standard for DC residential power systems,” *IEEE Trans. on Industry Applications*, vol. 58, no. 2, pp. 1446–1455, 2022.
- [10] M. R. K. Rachi and I. Husain, “Design and development of a hybrid DC circuit breaker for 380V DC distribution system,” in *Proc. 2021 IEEE Applied Power Electronics Conference and Exposition*, Phoenix, AZ, USA, 2021, pp. 1122–1127.
- [11] L. Kong, C. Li, J. Jiang, and M. G. Pecht, “Li-Ion battery fire hazards and safety strategies,” *Energies*, vol. 11, no. 9, #2191, 2018.
- [12] S. Saxena, L. Kong, and M. G. Pecht, “Exploding E-cigarettes: A battery safety issue,” *IEEE Access*, vol. 6, pp. 21442–21466, 2018.
- [13] D. P. Finegan, E. Darcy, M. Keyser *et al.*, “Identifying the cause of rupture of Li-Ion batteries during thermal runaway,” *Advanced Science*, vol. 5, no. 1, 1700369, 2018.
- [14] P. G. Balakrishnan, R. Ramesh, and T. P. Kumar, “Safety mechanisms in lithium-ion batteries,” *Journal of Power Sources*, vol. 155, no. 2, pp. 401–414, 2006.
- [15] Z. Ren, Y. Tong, Y. Liu, and G. Liu, “Load modeling and scheme design of 48V DC power supply system for civil buildings,” in *Proc. 2019 IEEE 3rd International Electrical and Energy Conf.*, Sep. 2019, pp. 1513–1517.
- [16] S. Zhao, F. Wu, L. Yang, L. Gao, and A. F. Burke, “A measurement method for determination of dc internal resistance of batteries and supercapacitors,” *Electrochemistry Communications*, vol. 12, no. 2, pp. 242–245, 2010.

Copyright © 2023 by the authors. This is an open access article distributed under the Creative Commons Attribution License (CC BY-NC-ND 4.0), which permits use, distribution and reproduction in any medium, provided that the article is properly cited, the use is non-commercial and no modifications or adaptations are made.



**Ke Liu** received the B.S. and M.S. degree in communication engineering from Shanghai University, Shanghai, China, in 2016 and 2019. She is currently working toward the Ph.D. degree in communication engineering with the graduated school of engineering, Tohoku University, Sendai, Japan. Her research interests include DC microgrid, smart grids, and power network.



**Hirohito Yamada** received the B.E. degree from Kanazawa University, Kanazawa, Japan, in 1981, and the M.E. and Ph.D. degrees from Tohoku University, Sendai, Japan, in 1983 and 1987, respectively, all in electronics engineering. In 1987, he joined the Opto-Electronics Research Laboratories, NEC Corporation, where he studied laser diodes for optical communications. Since 2006, he has been a Professor in the Department of Electrical and Communication Engineering, and International Research Institute of Disaster Science from 2022, Tohoku University, Sendai.



**Katsumi Iwatsuki** received the B.E. degree in electronics engineering from the Nagoya Institute of Technology, Nagoya, Japan, in 1981, and the M.E. and Ph.D. degrees in electronics engineering from the University of Tokyo, Tokyo, Japan, in 1983 and 1986, respectively. In 1986, he joined NTT Laboratories, where he engaged in research and research management related to optical communication system design and system performance evaluation, and open innovation through industry-academia collaboration. Since 2012, he has been a specially appointed professor of Research Organization of Electrical Communication in Tohoku University, where he engaged in coordinating and promoting the research collaboration project concerning “Disaster-Resistant Information Communication Network”. In 2022, he moved to International Research Institute Disaster Science in Tohoku University, where he worked on the planning and research and development of Resilience ICT-related R & D projects. He is the author or co-author of more than 210 papers and letters in technical journals and international conferences. He was active in the IEICE’s Technical Committee on Microwave and Millimeter-wave Photonics from 2013 to 2015. Some of his recent activities include Committee member of Asia-Pacific Microwave Photonics Conference 2012, TPC member of the 30th and 31st Progress In Electromagnetics Research Symposium (PIERS), and session organizer of “Microwave/Terahertz Photonics Technologies and their Applications” in PIERS (2007–2011). He received the Young Engineer’s Award from IEICE in 1991, the APCC/IEEE ComSoc APB Joint Award in 2001, and the European Microwave Conference Prize in 2006. He is a member of IEICE.



**Taiichi Otsuji** (Fellow, IEEE) received the B.S. and M.S. degrees in electronic engineering from the Kyushu Institute of Technology, Fukuoka, Japan, in 1982 and 1984, respectively, and the Ph.D. degree in electronic engineering from the Tokyo Institute of Technology, Tokyo, Japan, in 1994. He has been a professor at the Research Institute of Electrical Communication since 2005, and at the International Research Institute of Disaster Science since 2022, Tohoku University, Sendai, Japan. He has authored or co-authored more than 270 peer-reviewed journals. His current research interests include terahertz electronic, photonic, and plasmonic materials and devices and their applications for sustainable and resilient societies. Since 2013, he has been a Distinguished Lecturer with Electron Device Society, IEEE. He is a Fellow of the OPTICA and the Japan Society of Applied Physics, and a Senior Member of the Institute of Electronics, Information, and Communication Engineers (IEICE) of Japan, and a Member of the Materials Research Society, and the International Society for Optics and Photonics. He was the recipient of the Outstanding Paper Award of the 1997 IEEE GaAs IC Symposium, Prizes for Science and Technology (Research Category), the Commendation for Science and Technology by the Ministry of Education, Culture, Sports, Science and Technology, Japan, in 2019, and the 59th Achievement Award of the IEICE, Japan, in 2022.